

# Photoemission Phenomena on CEBAF RF Windows at Cryogenic Temperatures\*

T. Powers, P. Kneisel and M. Vaidya  
Continuous Electron Beam Accelerator Facility  
12000 Jefferson Avenue, Newport News, Virginia 23606 USA

## Abstract

This paper reports on the photoemission observed during the tests on a single-cell 1500 MHz niobium cavity with a polycrystalline alumina rf interface window operated at 2 K. The light emission from the window at 2 K was detected using a multi-channel fiber optics/PMT system and recorded with a 100 Ms/sec acquisition system. The spectral composition of two types of discharges has been measured. The results indicate that both broadband and narrow-band emissions are present, depending on the discharge type.

## I. INTRODUCTION

The CEBAF accelerator system uses 338 superconducting niobium cavity assemblies at 2 K to provide a continuous electron beam of 200  $\mu$ A and 4 GeV after 5 recirculations through 2 anti-parallel linear accelerators. Each cavity is equipped with a ceramic rf window located in the input coupler waveguide 7.6 cm away from the beam axis. This window hermetically seals the sensitive superconducting surfaces against the waveguide guard vacuum in line with the 5 kW klystrons. The CEBAF rf windows are presently made from a high-purity (99.9%) polycrystalline aluminum oxide ( $Al_2O_3$ ) sheet of dimensions 13.3 cm  $\times$  2.5 cm  $\times$  0.4 cm thick, which is brazed to a thin niobium foil frame that is in turn electron beam welded to a solid niobium frame for connection to the waveguide system in a bolted flange joint. This window design satisfies the requirements for operation at the machine's design values of an accelerating gradient of  $E_{acc} = 5$  MV/m and a  $Q$  value of  $Q \geq 2.4 \times 10^9$ . At higher gradients, however, several unwanted features such as surface flashover at the ceramic window or possible arc-induced vacuum leaks have been observed, especially in the presence of heavy field emission loading in the cavity [1].

Arcing phenomena at ceramic rf windows, especially when operating at room temperature with high peak power levels, have been previously observed: Y. Saito [2] reported characteristics of alumina windows operated in an S-band resonant ring configuration. Best power handling capabilities were obtained on alumina with high resistivity and a dense microstructure; the window failures were caused by multipacting electrons impinging on the ceramic surfaces with a secondary electron emission coefficient  $> 1$ . As a pre-breakdown phenomenon, broadband optical emission centered at 300 nm and 700 nm with a narrow emission line located at 694 nm has been observed and is interpreted as cathodoluminescence due to electron bombardment. More recently, spectroscopic observations of surface flashover on alumina under pulsed excitation revealed that the light spectrum contained not only lines due to gas desorption during the arcing but also aluminum oxide bands [3]. This

observation suggests that not only desorbed gases but also bulk material excitations from the specimen may contribute to the initiation of the surface flashover plasma.

## II. EXPERIMENTAL TEST SETUP

For the experiments reported in this paper, an end cell of a 5-cell cavity with a fundamental power coupler waveguide (FPC) was modified into a single-cell cavity (see figure 1) by the addition of a beam pipe. Cut-off tubes with flanges were electron beam welded to the FPC and the coax-to-waveguide adapter (tophat), permitting one to view the ceramic rf window from both sides through sapphire or quartz windows. Additionally, the interior of the cavity was monitored via a view port attached at the lower beam pipe. The entire cavity assembly was immersed in liquid He at 2 K.

The light produced in the cavity, beam pipe or FPC was transmitted from each of the view ports to the external environment at room temperature using a non-coherent bundle of 37 commercial grade 1 mm diameter acrylic fibers. The transmission characteristics of a 10 m section of fiber were measured at room temperature, 4.2 K and 2.0 K. The ratio of input to output optical signal was between 10% and 30% from 350 nm to 720 nm with no measurable change when 5 m of the fiber was cooled. Outside of the cryostat the light signal from each fiber bundle was split into 10 individual channels by means of an optical splitter which insured a uniform light input was provided to each of ten S-20 characteristic photomultiplier tubes. Using narrow band (10 nm FWHM) optical filters, which were placed between the individual fibers and nine of the calibrated photomultiplier tubes, it was possible to measure the temporal characteristics of the spectrum of the arcing phenomena.

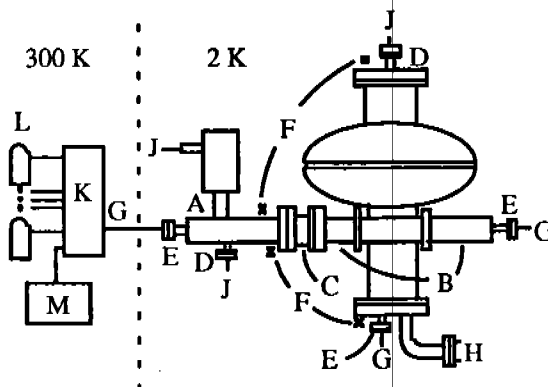


Figure 1. Diagram of a single-cell cavity showing (A) top hat with variable coupler, (B) fundamental power coupler, (C) ceramic window, (D) field probe locations, (E) optical windows, (F) x-ray detectors, (G) fiber optic bundles, (H) cavity pump-out port, (J) rf cables, (K) optical splitter, (L) photomultiplier/filter assembly and (M) monochromator.

\*This work supported by DOE Contract DE-AC05-84ER40150

During the experiments the cavity was typically operated at a peak surface field of 22 to 25 MV/m with field emission loading producing  $> 100$  Rad/hr at the cavity. Field levels in the cavity and the window-waveguide space were measured by means of pickup probes located at the beam pipe and tophat, respectively. Silicon photodiodes (Hamamatsu A1221-01) were used as X-radiation detectors [4]. They were placed on the cavity window frame and at the beam pipes. The transfer function of the 20 kHz BW signal conditioning amplifier was  $15 \text{ V}/\mu\text{A}$ . It has been empirically determined that the output voltage of this amplifier detector combination is on the order of  $10 \text{ Rad/hr-mV}$  [1].

Data acquisition was provided by four 100 Ms/s digital oscilloscopes with a total of 12 channels. Typical sample rates were 20 Ms/s with a record length of 1000 points. The PMT signal, which was not optically filtered, was used by a detection circuit that provided a latched trigger signal when the PMT current was above a level, typically  $20 \mu\text{A}$ , for more than  $2 \mu\text{s}$ . This trigger signal simultaneously triggered all acquisition channels. The data were transferred via IEEE-488 protocol to a Macintosh computer for storage, and the arc detection circuitry was reset automatically using the LabVIEW® software package.

### III. RESULTS AND DISCUSSION

#### A. Types of arcing phenomena

Two types of light-emitting events will be discussed in this paper. In both types of events the energy stored in the cavity disappears several orders of magnitude faster than the 80 ms decay time of a cavity with a  $Q_L$  of  $10^9$ . In one type of event which has recently been identified [1, 5], the stored energy, as measured by the transmitted power signal, is fully dissipated in less than  $5 \mu\text{s}$ . Decay times as short as 150 ns have been measured. This is accompanied by a large, short duration X-ray pulse of approximately 500 kRad/hr for less than  $5 \mu\text{s}$  and a short intense light pulse which is detected at the beam pipe and on both the cavity and waveguide side of the ceramic window. Typical rf and photomultiplier signals for this type of event are shown in figure 2. This class of phenomena, which we call "electronic quenches," are interpreted as the effects produced by the sudden injection or liberation of a large number of electrons into the cavity. The electrons and their secondaries quickly absorb the rf energy stored in the cavity and produce an intense bremsstrahlung pulse as they strike the cavity wall, beam pipe, or endplate. This "beam" loading of the cavity is consistent with the effects seen at DESY when a superconducting cavity is heavily beam loaded [6].

In the second type of event, the cavity stored energy is dissipated in several hundred microseconds (typically  $500 \mu\text{s}$ ). Figure 3 is an example of this type of event. The field level in the tophat is extinguished in a few hundred nanoseconds, but it starts to build up again as the stored energy is drained from the cavity. When the cavity energy reaches a minimal level the field in the tophat collapses and the discharge is extinguished. This type of event is interpreted as a discharge occurring in the window/tophat region which is sustained by the stored energy in the cavity. The light emission during this type of discharge has three different temporal phases. During the first  $50 \mu\text{s}$  a relatively large light pulse, which has the

same temporal and spectral characteristics as that of an electronic quench, is observed. For the next  $350 \mu\text{s}$  an emission, which has distinctly different spectral characteristics from an electronic quench, is observed. This is followed by a long tail, which has similarities to the long decay tail of the electronic quench.

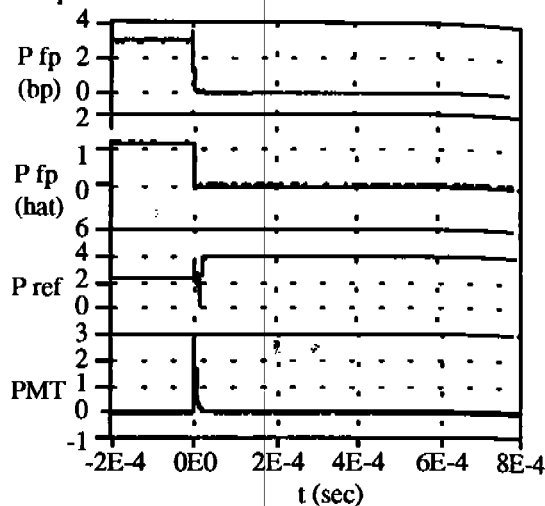


Figure 2. Beam pipe rf probe, tophat rf probe, reflected power and PMT signals for an electronic quench (vertical units are arbitrary).

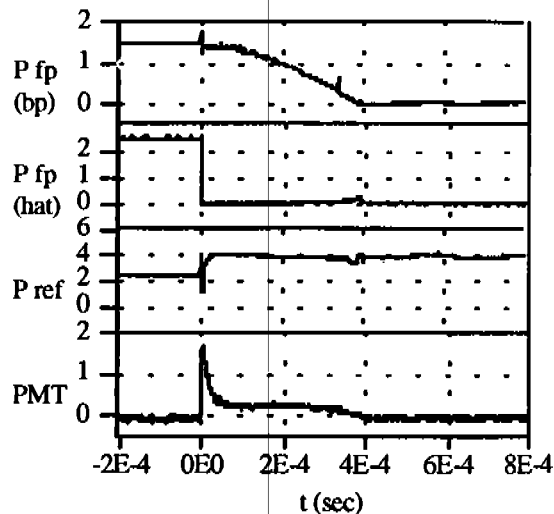


Figure 3. Beam pipe rf probe, tophat rf probe, reflected power and PMT signals for a window/tophat discharge (vertical units are arbitrary).

#### B. Spectral characteristics

The optical emission data were extracted from the raw data as follows. The average value of the photomultiplier tube current for different temporal regions of the discharges was calculated. These values were scaled by the tube and filter attenuation factors. The ratio between the channel in question and the output of the unfiltered photomultiplier tube for the same section of the waveform was calculated. Several data points were calculated for each filter value and temporal region of the different discharge types and averaged. Typically, the spread in the data was 20 percent of the value shown in the graphs. In total 200 discharge events were used to generate the results reported in this paper.

As shown in figure 4a, for the first 50  $\mu\text{s}$  of both types of events the spectral responses are almost identical. Preliminary studies with a monochromator indicate that the large emission peak occurs at  $394.2 \pm 1$  nm. We suspect that this line is a solid state line associated with the ceramic material. However, this is yet to be confirmed. The next spectral type was measured during the period of time between 50  $\mu\text{s}$  and 400  $\mu\text{s}$  on a window/tophat discharge (see figure 4b). This temporal region of the discharge is characterized by several

different peaks covering the entire spectrum measurable with the current optical fibers. Analysis of this data will be performed when better diagnostics become available. The final two spectral data plots, which are combined in figure 4c, represent the data taken during the long (tens of milliseconds) decay tails. Although they are different they both contain a strong line between 685 nm and 695 nm. Other researchers [2, 7] have reported on a line at 694 nm, identifying it as a chromium impurity level in alumina. In our experimental setup this line could originate in the ceramic window or at the sapphire view ports.

#### IV. CONCLUSIONS

The experimental investigations reported here are preliminary tests to understand the arcing phenomena encountered when ceramic rf window materials are operated at cryogenic temperatures. It is obvious that this phenomenon is very complex, involving both solid state processes in the ceramic material and probably desorption processes at the cryogenic surfaces under the influence of ionizing and optical radiation. Existing data from dc-pulsed and rf experiments indicate that the microstructure and impurity content of the material as well as the surface conditions influence the flashover characteristics. It is believed that temporal spectral data of the surface flashover phenomena will help to untangle the complex nature of this phenomenon, which can become a serious impediment to the operation of an accelerator with cavities run well into field emission. Future work involves the use of a spectrometer and a gateable detector array to further resolve the temporal and spectral information to try to identify the initiating mechanisms associated with the discharge process.

#### V. REFERENCES

- [1] T. Powers, *et al.*, "RF Window Arcing Studies Update, A Comparison of Results from Cryomodule 17 and Vertical Cavity Testing," CEBAF TN93-030.
- [2] Y. Saito, *et al.*, "Breakdown of Alumina RF Windows," *IEEE Trans. on Electrical Insulation*, 24 (6), 1029—1032 (1989).
- [3] T. Sudarshan, *et al.*, "Spectroscopic Observations of Surface Flashover Across an Insulator in Vacuum Under Pulse Excitation," to be published.
- [4] B. Fischer, "Untersuchungen an Supraleitenden 9-zelligen Prototyp Resonatoren für TESLA," Report University of Wuppertal, Fachbereich Physik, July 1992, Wuppertal, Germany.
- [5] L. Phillips, *et al.*, "Some Operational Characteristics of CEBAF RF Windows at 2 K," in proceedings of this conference.
- [6] Y. Sekutowicz, private communication.
- [7] K. Lee, *et al.*, "Luminescence of the F Center in Sapphire," *Phys. Rev.* 19 (6), 3217—3221 (March 1979).

#### VI. ACKNOWLEDGMENTS

We would like to thank Bret Lewis, Pete Kushnick, Carl Zorn and the cryogenic support team for their effort in the work described in this paper.

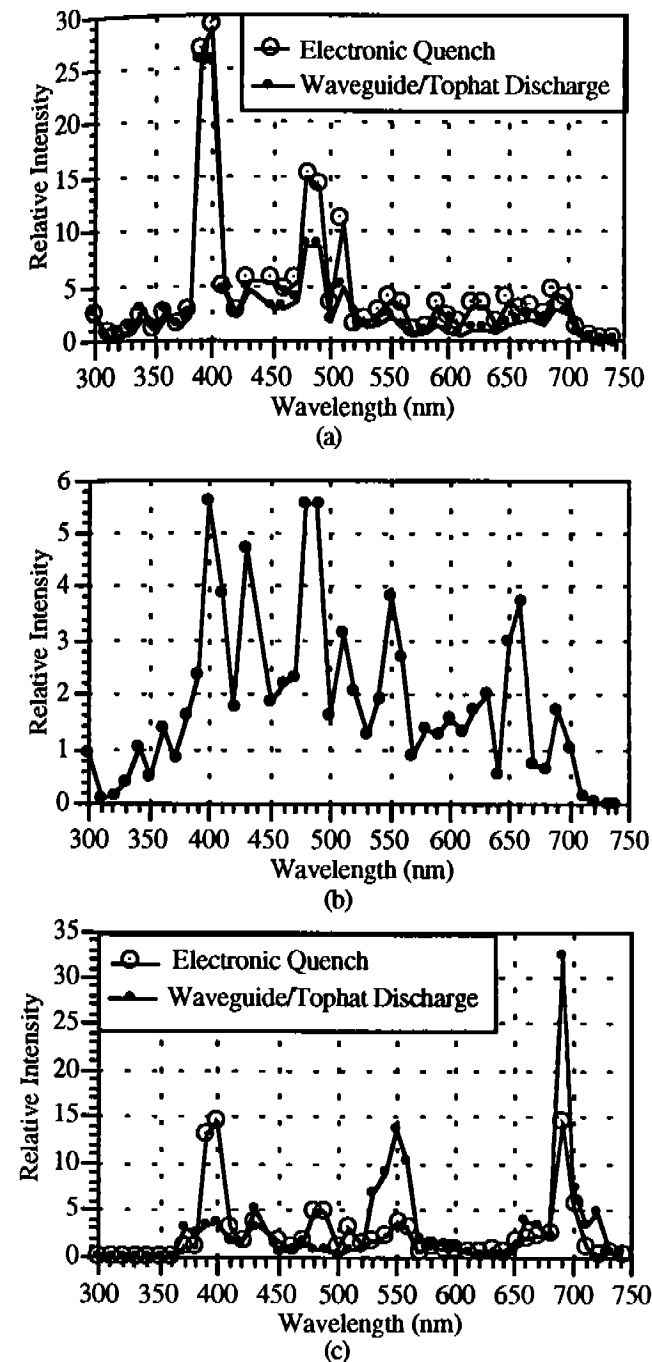


Figure 4. Spectral characteristics of different temporal regions of the two different discharge types. (a) First 50  $\mu\text{s}$  of both the electronic quench and waveguide/tophat discharge. (b) Second temporal region for a waveguide/tophat discharge  $50 \mu\text{s} < t < 400 \mu\text{s}$ . (c) Last 400 to 600  $\mu\text{s}$  of both an electronic quench and a waveguide tophat discharge.